[3]R. Landauer, IBM J. Res. Develop. 1, 223 (1957).
[4]R. Landauer, in Report to the Sponsors of the International Conference of the Electronic Properties of Metals at Low Temperatures, Hobart College, 1958, p. 173 (unpublished). These conference proceedings were given a limited distribution. Copies of the particular paper cited here are available from the author upon request.
[5]R. Landauer, Phil. Mag. 21, 863 (1970).
[6]H. B. Huntington, Trans. AIME 245, 2751 (1969).
[7]F. M. d'Heurle, Proc. IEEE 59, 1409 (1971).
[8]V. Ambegaokar, B. I. Halperin, and J. S. Langer, Phys. Rev. B 4, 2612 (1971); S. Kirkpatrick, Phys. Rev. Letters 27, 1722 (1971).

PHYSICAL REVIEW B VOLUME 5, NUMBER 4 15 FEBRUARY 1972

Higher-Derivative Photoemission Spectra and the Relativistic Band Structure of Gold

Neville V. Smith
Bell Laboratories, Murray Hill, New Jersey 07974
(Received 7 September 1971)

Following a prescription by Ehrenreich and Hodges, a relativistic band structure for Au has been constructed by the insertion of spin-orbit coupling into an originally nonrelativistic interpolation scheme. The bands are used to compute the energy distribution of the joint density of states $D(E, \hbar\omega)$ and its second derivative with respect to energy $D''(E, \hbar\omega)$. Peaks in $-D''(E, \hbar\omega)$ are found to correlate quite well in energy location with structure in experimental higher-derivative photoelectron-energy spectra measured on cesiated Au. The comparison is made with previous data and with supplementary spectra presented here. Profile changes in the experimental spectra on varying the photon energy $\hbar\omega$ are also reasonably well accounted for. The density of states computed from the same band structure shows d-band peaks at 2.65, 4.00, 4.50, 5.05, 6.35, 6.85, and 7.60 eV below the Fermi level. From the derivative spectra at the lower photon energies, the $L_6^-(L_{2'}) \rightarrow L_6^+(L_1)$ band gap in Au is estimated to be 4.0 eV.

I. INTRODUCTION

Several relativistic band calculations on Au have been performed recently,[1-3] and they confirm that relativistic effects are quite large in a heavy element such as Au. Experimental information from optical and photoemission studies is now sufficiently detailed that the relativistic effects should be taken into account in any realistic interpretation. Christensen and Seraphin[1] have laid particular emphasis on this point, and it has been considered also by Kupratakuln.[2] Indeed, an attempt made in an earlier paper by the author[4] to interpret the photoemission spectra of Au using a nonrelativistic band structure was significantly less successful than similar analyses on the lighter metals Cu and Ag.

This paper presents a reanalysis of the photoemission data from Au using an interpolated band structure into which spin-orbit coupling has been inserted. It is assumed that the relativistic effects other than spin-orbit coupling (mass-velocity and Darwin terms) can be absorbed into the parameters of the original nonrelativistic interpolation scheme. In fact, we follow very closely the prescription set down by Ehrenreich and Hodges.[5] The interpolated band structure is used to compute the energy distribution of the joint density of states (EDJDOS) and its second derivative with respect to energy. These results are then compared with higher-derivative photoelectron-energy spectra taken on cesiated Au. It is found that the inclusion of spin-orbit splitting does bring about a significant improvement in agreement with experiment and permits a more reliable identification of structure. Good agreement for photon energies greater than about 9.0 eV has been reported also by Christensen,[6] who has computed the EDJDOS from a relativistic augmented-plane-wave (APW) calculation.

New higher-derivative photoelectron-energy spectra on cesiated Au are presented here in order to supplement those presented in the earlier paper,[4] particularly in the lower photon-energy region. The new spectra show some interesting profile changes on varying the photon energy. It is shown that these are also consistent with the predictions of the interpolated band structure.

II. BAND STRUCTURE OF GOLD

A. Interpolation Scheme

The band structure used here is obtained from the interpolation scheme of Hodges, Ehrenreich, and Lang[7] (HEL). As pointed out by them and by Ehrenreich and Hodges,[5] the original nonrelativistic HEL scheme can be converted into a relativistic scheme in an approximate manner by expressing the model Hamiltonian as follows:

$$H=\begin{bmatrix} H_{cc} & H_{cd} & 0 & 0 \\ H_{dc} & H_{dd}+\xi M & 0 & \xi N \\ 0 & 0 & H_{cc} & H_{cd} \\ 0 & -\xi N^* & H_{dc} & H_{dd}+\xi M^* \end{bmatrix} . \quad (1)$$

H_{cc}, H_{cd}, H_{dc}, and H_{dd} are the blocks of the 9×9 model Hamiltonian of the original HEL scheme; H_{cc} is the 4×4 orthogonalized-plane-wave (OPW) block; H_{dd} is the 5×5 tight-binding d-d block as worked out by Fletcher[6]; H_{cd} and H_{dc} are the hybridization blocks. This matrix is doubled up to form the 18×18 matrix. Spin-orbit coupling is included by the insertion of the 5×5 matrices M, M^*, N, and $-N^*$, as shown, which couple the d-d blocks of opposite spin. The matrices M and N, taken by Ehrenreich and Hodges from the previous work by Friedel *et al.*[9] and by Abate and Asdente,[9] are given by

$$M=\frac{i}{2}\begin{bmatrix} 0 & ss' & -sc' & 2c & 0 \\ -ss' & 0 & c & -sc' & -3^{1/2}sc' \\ sc' & -c & 0 & -ss' & 3^{1/2}ss' \\ -2c & sc' & ss' & 0 & 0 \\ 0 & 3^{1/2}sc' & -3^{1/2}ss' & 0 & 0 \end{bmatrix}, \quad (2)$$

$$N=\frac{1}{2}\begin{bmatrix} 0 & c'+ics' & s'-icc' & -2is & 0 \\ -(c'+ics') & 0 & -is & s'-icc' & 3^{1/2}(s'-icc') \\ -(s'-icc') & is & 0 & -(c'+ics') & 3^{1/2}(c'+ics') \\ 2is & -(s'-icc') & (c'+ics') & 0 & 0 \\ 0 & -3^{1/2}(s'-icc') & -3^{1/2}(c'+ics') & 0 & 0 \end{bmatrix}, \quad (3)$$

where $c=\cos\theta$, $s=\sin\theta$, $c'=\cos\varphi$, $s'=\sin\varphi$, and where θ and φ define the direction of spin quantization which, in these calculations, was taken arbitrarily at $\theta=\pi/2$ and $\varphi=\pi/2$.

The spin-orbit coupling parameter ξ was set equal to 0.0485 Ry. This value was taken from the work of Connolly,[3] and is somewhat less than the atomic value of 0.053 Ry deducible from Herman and Skillman's tables.[10] The values of the other parameters of the HEL scheme are shown in Table I. These were obtained by fitting an adjusted version of Ballinger and Marshall's nonrelativistic band calculation.[11] The details of the adjustments are described in an earlier paper[4] and are mentioned briefly below. The Fermi level E_F, also shown in Table I, is slightly different from that given elsewhere.[4,11] The new value gives better agreement with photoemission as regards the depth of the uppermost d bands.

So far we are following exactly the procedure recommended by Ehrenreich and Hodges.[5] The only modification we have introduced into their scheme concerns the so-called symmetrizing factors F_2, F_3, and F_4. At points of high symmetry, these take the values of 0 or 1, depending on whether the associated plane waves are excluded or included in the correct symmetrized combination. The expressions for the F's we have used are as follows[12]:

$$F_2=\sin^2\left(\frac{\pi}{2}\,\frac{k_y-k_x}{16-k_x-k_y}\right), \quad (4)$$

$$F_3=\sin^2\left(\frac{\pi}{2}\,\frac{k_x+k_z}{12-k_y}\right), \quad (5)$$

$$F_4=\sin^2\left(\frac{\pi}{2}\,\frac{k_x-k_z}{12-k_y}\right). \quad (6)$$

These F's perform somewhat better than those proposed by Ehrenreich and Hodges.[5] The reasons for our choice are discussed in the Appendix.

The energy eigenvalues obtained by diagonalization of the model Hamiltonian are illustrated for a few important symmetry directions in Fig. 1. Splittings due to spin-orbit coupling are in excess of 1 eV and are therefore appreciably greater than

TABLE I. Parameters of the interpolated band structure of Au (energies are in rydbergs).

d bands	
A_1	0.039 38
A_2	0.010 63
A_3	0.020 03
A_4	0.026 28
A_5	0.005 31
A_6	0.017 08
E_0	−0.357 50
Δ	−0.025 12
4 OPW	
V_{111}	0.103 87
V_{200}	0.155 16
α	0.013 83
β	−0.620 00
Hybridization	
B_1	0.57
B_2	1.16
Spin orbit	
ξ	0.048 5
Fermi level	
E_F	−0.014 7

the typical resolution of photoemission experiments (~ 0.2 eV).

Only spin-orbit coupling has been inserted explicitly. In the spirit of the interpolated-band approach, it is assumed that the other relativistic effects (mass-velocity and Darwin terms), although not small, can somehow be absorbed into the parameters of the existing nonrelativistic scheme. One possible instance of this concerns the gap between the conduction bands at L. The levels on each side of the gap are referred to as L_6^- and L_6^+ in the double-group notation and correspond to the levels L_2' and L_1 in the nonrelativistic case. In obtaining the parameters of the HEL scheme (shown in Table I) by fitting Ballinger and Marshall's nonrelativistic bands, [11] the author lowered the L_1 level by 0.14 Ry. This large arbitrary adjustment was considered necessary in order to bring the $L_{2'} \rightarrow L_1$ gap into closer agreement with the optical value. Kupratakuln[2] has pointed out that nonrelativistic calculations tend to overestimate the $L_{2'} \rightarrow L_1$ gap. The large downward adjustment of L_1 is therefore not as arbitrary as it first appeared, since it may represent a crude relativistic correction. Spin-orbit coupling, however, cannot be absorbed in this way, since it lifts degeneracies and brings about a qualitative modification of the bands.

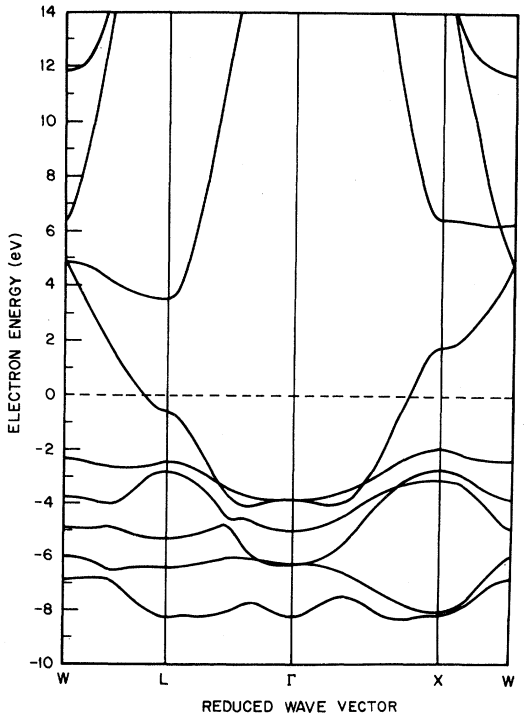

FIG. 1. Interpolated-band structure of gold. The zero of energy is taken at the Fermi level.

B. Energy Distribution of Joint Density of States

Having set up a model band structure, let us now consider its predictions with regard to photoemission experiments. Assuming that the optical transitions are direct ($\vec{k}$ conserving), a property of the band structure to which we expect the photoelectron-energy spectra to bear a resemblance is the energy distribution of the joint density of states (EDJDOS) defined by[13]

$$D(E,\hbar\omega)=\sum_{f,i}\int_{BZ} d^3k\,\delta(E_f-E_i-\hbar\omega)\delta(E-E_i)\ . \tag{7}$$

$E_f(\vec{k})$ and $E_i(\vec{k})$ denote the energies at $\vec{k}$ in a final band f and an initial band i, respectively. The first δ function imposes the energy- and wave-vector-conservation restrictions. The second δ function selects out those direct transitions whose initial-state energy equals our specified value E.

The EDJDOS is not the photoelectron-energy spectrum itself, but represents merely the total number of direct transitions which can take place at photon energy $\hbar\omega$ from states of energy E. To obtain the true spectrum, each transition should be weighted by the square of a momentum matrix element[14] and by an over-all escape factor.[14,15] These weighting factors will distort the spectrum from the EDJDOS by, for example, changing relative peak heights, and by suppressing some peaks altogether. The spectrum is also likely to be riding on a background consisting of scattered electrons,[15,16] possible contributions due to nondirect transitions,[15,16] and to a variety of surface photoelectric mechanisms.[17] Computations reveal that the EDJDOS contains much pronounced structure. Our interpretation in terms of the EDJDOS rests upon the assumption that some of this structure will survive the distortions and degradations mentioned above and be identifiable in the experimental spectra.

The EDJDOS was evaluated by a histogram method similar to that described in the earlier paper.[4] It involved sampling 97000 $\vec{k}$-space points arranged along a cubic mesh in the appropriate $\frac{1}{48}$-th wedge of the Brillouin zone. The model Hamiltonian was actually diagonalized at only 3100 points using the high-speed HECEVV routine described by Faulkner.[18] Linear interpolation was used for other points. Some of the numerical results are illustrated in Fig. 2, where we show the EDJDOS histogram for the photon energy interval $7.5 < \hbar\omega < 7.6$ eV.

The second derivative of the EDJDOS with respect to electron energy, namely,

$$D''(E,\hbar\omega)\equiv\frac{\partial^2 D(E,\hbar\omega)}{\partial E^2}\ , \tag{8}$$

was computed by a finite-difference method from

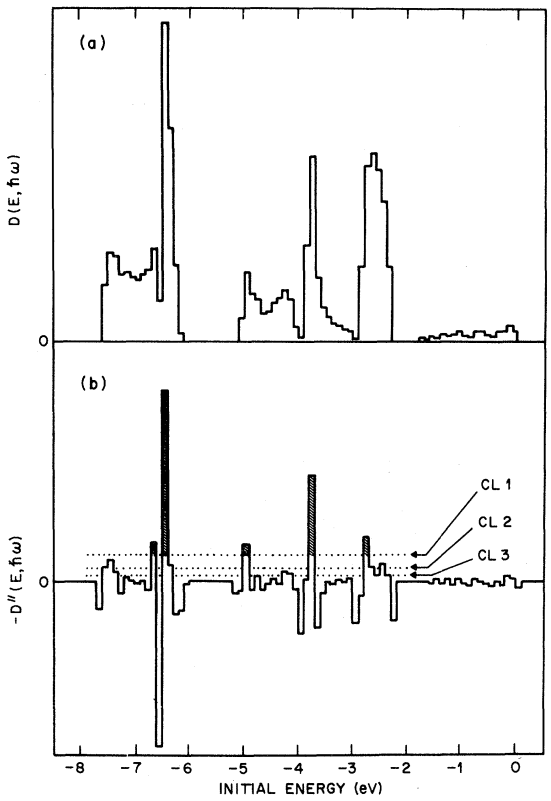

FIG. 2. The EDJDOS for Au in the photon-energy interval $7.5 < \hbar\omega < 7.6$ eV; (a) $D(E, \hbar\omega)$, the EDJDOS itself; (b) $-D''(E, \hbar\omega)$, the negative of the second derivative of the EDJDOS with respect to electron energy.

the EDJDOS histogram. This was considered desirable since we will eventually be comparing the band-structure predictions with higher-derivative experimental spectra. If h_n represents the height of the EDJDOS histogram in the nth energy interval, then the $D''(E, \hbar\omega)$ histogram is given by $h_{n+1} - 2h_n + h_{n-1}$. The histogram for $-D''(E, \hbar\omega)$ is also shown in Fig. 2(b). We choose to consider $-D''$ rather than $+D''$ in order to bring out the rough peak-for-peak correspondence between $-D''(E, \hbar\omega)$ and $D(E, \hbar\omega)$.

The behavior of $D(E, \hbar\omega)$ and $-D''(E, \hbar\omega)$ as a function of $\hbar\omega$ is illustrated in Figs. 3 and 4. Figures 3(a) and 4(a) show a succession of smoothed EDJDOS curves. These were obtained by convolving the $D(E, \hbar\omega)$ histograms with a Lorentzian broadening function whose full width at half-maximum was 0.3 eV. Figures 3(b) and 4(b) show a corresponding set of smoothed $-D''(E, \hbar\omega)$ curves obtained by using the same broadening function. We note that, for a given value of the broadening, the derivative spectra offer more structural detail than the ordinary spectra. Some of the peaks in Figs. 3 and 4 have been labeled with numbers. This is in anticipation of certain identifications we will be making later in the paper.

An alternative way of summarizing large numbers of $-D''(E, \hbar\omega)$ spectra is to construct the coarse contour map shown in Fig. 5. The histogram intervals on the E and $\hbar\omega$ scales are 0.1 eV. Different symbols are used to denote various levels in the contents of the histogram bins. Large peaks are denoted by the symbol "○" and these correspond to contributions which rise above the contour level CL1 indicated in Fig. 2(b). The symbol "×" denotes contributions falling between contour levels CL2 and CL1; and "◆" denotes contributions between levels CL3 and CL2, again indicated in Fig. 2(b). Contributions whose heights fall below contour level CL3 are not shown.

We have therefore arrived at a prediction for the way in which the profile of the photoelectron-energy spectrum should change on varying the photon energy. It is to be noted that plotting the loci of peaks in the EDJDOS itself would give a diagram not very different from that shown in Fig. 5. What differences there are arise mostly from the approximate nature of the peak-for-peak correspondence mentioned above and elsewhere.[4] Peaks in $D(E, \hbar\omega)$ give rise to peaks in $-D''(E, \hbar\omega)$. However, the reverse is not always true. Peaks in $-D''(E, \hbar\omega)$ can arise also from *edges* in $D(E, \hbar\omega)$. Edges are to be expected from some of the two-dimensional critical points which characterize this problem.[19]

III. COMPARISON BETWEEN THE BANDS AND EXPERIMENT

A. Higher-Derivative Photoelectron-Energy Spectra

Before proceeding to the comparison between the EDJDOS calculations and experiment, we present here some new higher-derivative photoelectron-energy spectra taken on cesiated Au. These supplement the spectra presented in the earlier paper,[4] particularly in the lower-photon-energy region. The spectra were measured by the same technique of using the conventional ac-modulated retarding-potential technique[20] and tuning in on the third harmonic of the ac photocurrent rather than the first.[21] For sufficiently small values of the amplitude of the ac-modulating voltage (0.3 V peak to peak was used here), these spectra are proportional to the second derivative of the photoelectron-energy distribution, namely,

$$N''(E, \hbar\omega) \equiv \frac{\partial^2 N(E, \hbar\omega)}{\partial E^2} \quad . \tag{9}$$

The advantage of the second-derivative spectra is that they accentuate structure and discard the smooth background. We will be plotting $-N''$ rather than N'', since peaks in N tend to give rise to peaks in $-N''$ at almost the same energy loca-

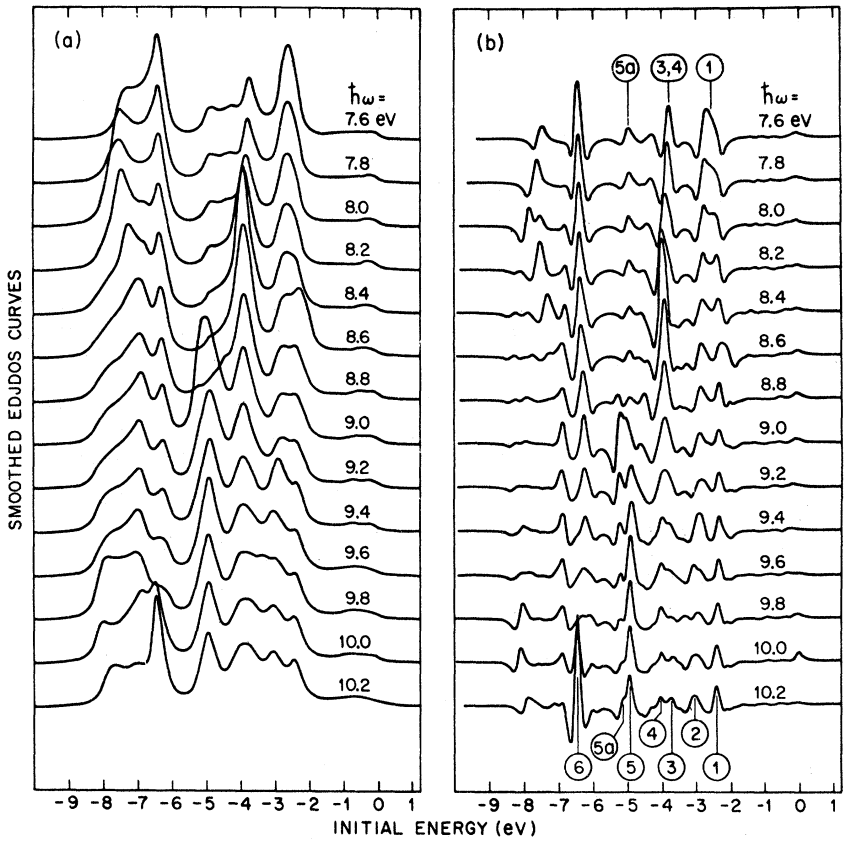

FIG. 3. Smoothed EDJDOS curves for Au in the photon-energy range 7.6–10.2 eV: (a) curves of $D(E, \hbar\omega)$; (b) curves of $-D''(E, \hbar\omega)$. A Lorentzian broadening function of 0.3 eV full width at half-maximum was used. The photon energies shown represent the upper limit of the 0.1-eV histogram interval.

tion. We will be referring the spectra to the initial-state energy in the usual way.[4]

Figure 6 shows the $-N''(E, \hbar\omega)$ spectra on cesiated Au in the photon-energy range 7.4–9.2 eV. Seven pieces of structure are observed and have been labeled 1, 2, 3, 4, 5, 5a, and 6. Peaks 1–6 correspond, respectively, to peaks B–G in the nomenclature of Nilsson *et al.*[22] These peaks are attributed to transitions from the *d* bands. The peak at the extreme-low-energy end of each spectrum is produced by scattered electrons and threshold effects and will be ignored. From Fig. 6 we extract the following three major points concerning the behavior of the spectra.

Point (*i*). A piece of structure labeled 2 is seen on the low-energy side of peak 1 at the higher photon energies. At even higher photon energies it diverges from peak 1 and becomes a separate peak. This latter feature has been adequately documented elsewhere[4,22,23] and is not illustrated further here.

Point (*ii*). Peaks 3 and 4, which are resolvable as a doublet at $\hbar\omega = 9.2$ eV, are observed to merge at lower photon energies and become a single peak at about $\hbar\omega = 7.4$–7.6 eV. This merging was discernible in the earlier paper[4] and has been observed also by Lindau and Walldén.[24]

Point (*iii*). Peak 5 undergoes some profile changes on varying $\hbar\omega$. At $\hbar\omega = 9.2$ eV there is a shoulder labeled 5a on its low-energy side. This shoulder fades away at lower photon energies (~ 9.0 eV), although it does not disappear completely since, even at $\hbar\omega = 9.0$ eV, peak 5 remains noticeably asymmetric. At even lower photon energies (~ 8.8 eV), peak 5 sharpens up, and the shoulder 5a reemerges. Eventually, at $\hbar\omega = 8.4$ eV, 5a becomes the dominant peak.

Figure 7 shows the behavior of $-N''(E, \hbar\omega)$ in the photon-energy range 5.8–7.4 eV. We extract from these data the following additional three major points.

Point (*iv*). The single peak formed by the merger of peaks 3 and 4 at around $\hbar\omega = 7.4$–7.6 eV undergoes further profile changes on proceeding to lower photon energies. First we observe a peak labeled 3a which branches off on the high-energy side.

Point (*v*). If we follow the same single peak mentioned above to lower photon energies, we find that around $\hbar\omega = 6.5$ eV it is observed to split again forming the two shoulders labeled 3b and 3c.

Point (*vi*). The leading peak labeled 1 develops

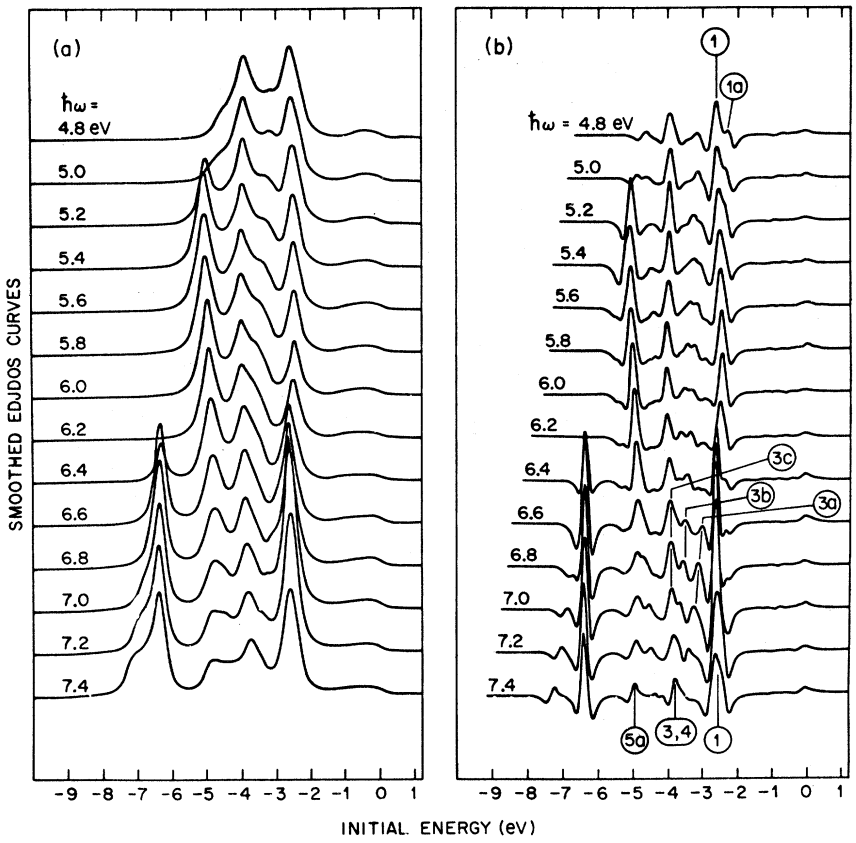

FIG. 4. Smoothed EDJDOS curves for Au in the photon-energy range 4.8–7.4 eV: (a) curves of $D(E, \hbar\omega)$; (b) curves of $-D''(E, \hbar\omega)$. A Lorentzian broadening function of 0.3 eV full width at half-maximum was used. The photon energies shown represent the upper limit of the 0.1-eV histogram interval.

a shoulder on its high-energy side which, at the lower photon energies, emerges as the separate peak labeled 1a. It should be mentioned that peak 1a is a peak only in the $-N''(E, \hbar\omega)$ spectrum. In the $N(E, \hbar\omega)$ spectrum it appears as a bulge on the high-energy edge of peak 1.

There are some other weaker pieces of structure in the spectra of Figs. 6 and 7 which we list in the following two minor points.

Point (vii). At $\hbar\omega = 8.2$ eV, there is a weak shoulder on the low-energy side of peak 4. At photon energies 7.4–8.0 eV there is a weak piece of structure in the valley between peaks 5a and 4.

Point (viii). At $\hbar\omega = 8.4$ eV, there is a weak peak in the valley between peaks 3 and 2. This persists down to $\hbar\omega = 7.4$ eV. At $\hbar\omega = 7.2$ eV, there is a weak shoulder between shoulder 3a and peak 1.

The existence of the structure listed in points (vii) and (viii) will not be stressed too strongly here for the following reason. The structure is weak and falls well below the zero line. A consideration of simple line shapes leads to the realization that two adjacent peaks in $N(E, \hbar\omega)$ will give rise to two peaks in $-N''(E, \hbar\omega)$, but that these peaks could be accompanied by a spurious intermediate peak below the zero line. We cannot rule out the possibility that the weak structure falls into this category. However, we would recommend further study of this structure since there are features in the calculated EDJDOS with which some of it could possibly be identified. Our emphasis here will be on the stronger structures listed in points (i)–(vi).

B. Comparison with the EDJDOS

The results of the experimental spectra and the numerical computations are summarized and compared in the structure plot of Fig. 8. The plotted circles represent the energy locations of structural features in the experimental spectra. Full circles denote positions of peaks, while open circles represent shoulders. We refer always to structure in the *derivative* spectra. A peak in the second-derivative spectrum does not always correspond to a peak in the ordinary spectrum, but may indicate an edge. Peak 1a, for example, seems to fall into this category. For consistency, therefore, we will be comparing $-N''(E, \hbar\omega)$ with $-D''(E, \hbar\omega)$. The curves in Fig. 8 represent the loci of peaks in $-D''(E, \hbar\omega)$. These were constructed by freehand tracing over the contour map

of Fig. 5. Full curves are intended to denote strong peaks. Broken curves denote weaker peaks.

The profile changes on varying $\hbar\omega$ in the experimental spectra of Figs. 6 and 7 and listed in points (i)–(vi) above show some correlation with the behavior of peaks in $-D''(E,\hbar\omega)$. The experimental peaks 1 and 2 evolve into peaks 1 and 1a at the lower photon energies. Similar behavior is seen in the peak loci of $-D''(E,\hbar\omega)$. The merging together of peaks 3 and 4 and their eventual evolution into the structures 3a, 3b, and 3c also find their counterparts in $-D''(E,\hbar\omega)$.

In addition to the agreement with regard to the qualitative behavior, there is also fairly good agreement for the actual energy locations of structure. At the higher photon energies, the six main peaks, 1–6, fall quite close to loci of peaks in $-D''$ with which they may therefore be identified. In this respect, the agreement is significantly better than that obtained previously by the author[4] using an interpolated fit to a nonrelativistic band structure.[25] In that work, the bands were chosen for their good agreement as far as position and width of the d bands were concerned, but it was found that the internal features of the d bands did not match up too well with experiment. Specifically, peaks 3–5 could not be unambiguously identified.[25] Of course, it might have been possible to adjust the parameters of the nonrelativistic scheme in order to force agreement with experiment. However, it is doubtful whether this could have been done without violating the interrelationships between the parameters required by the resonance formulation of the d bands.[26] Once the width of the d resonance has been fixed, one is not at liberty to make large arbitrary adjustments of the parameters describing the internal features of the d bands (in our case, the relative values of the Fletcher-Wohlfarth A_n parameters and also Δ).

Certain small changes of the parameters presented in Table I might be desirable. For example, while peaks 1–3 fall quite close to peak loci in $-D''$, peaks 4 and 5 fall at slightly lower energies than the peak loci in $-D''$ with which they have been identified. The discrepancy could be removed by a slight stretching of the d bands. This could be accomplished by increasing all the A_n's uniformly by a few percent, thus increasing the width of the d resonance. E_0, which is roughly the center of the resonance, would then have to be decreased slightly in order to restore the upper edge of the d bands to its correct position. One notes that while the theoretical curves of Figs. 3(b) and 4(b) reproduce much of the qualitative behavior of the

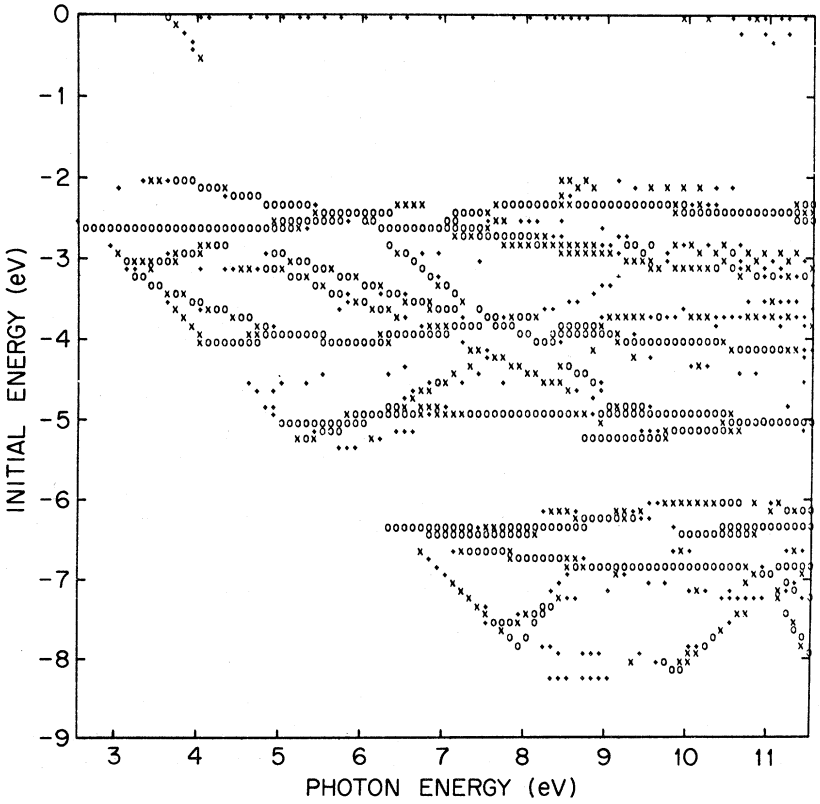

FIG. 5. Contour map of the $-D''(E,\hbar\omega)$ histogram. The symbol "O" represents histogram contributions rising above contour level CL1 indicated in Fig. 2(b); "×" represents histogram levels falling between contour levels CL1 and CL2 also shown in Fig. 2(b); "◆" represents contributions between levels CL2 and CL3.

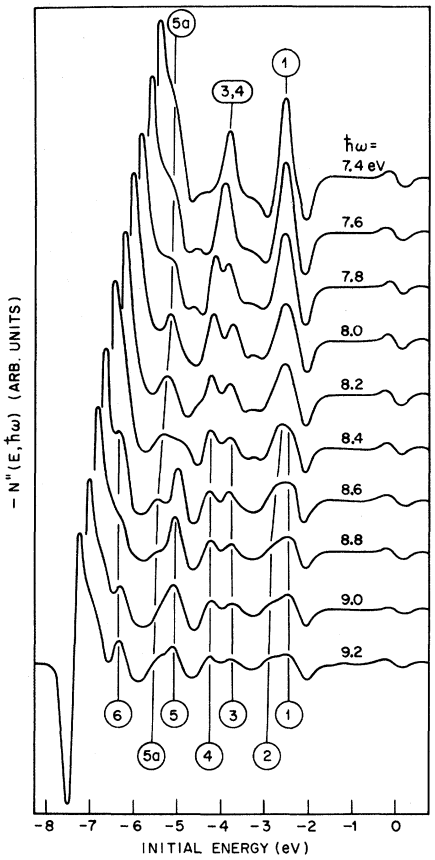

FIG. 6. Experimental higher-derivative photoemission spectra $-N''(E, \hbar\omega)$ taken on cesiated Au in the photon-energy range 7.4–9.2 eV.

evolution of structure in the experimental spectra, certain events such as peak splittings or mergings do not always occur at the correct photon energy. Small adjustments of the bands would possibly remedy these defects as well.

C. Density of States

The interpolated band structure was also used to calculate the ordinary density of states (DOS) defined by

$$\rho(E) = \sum_i \int_{BZ} d^3k\, \delta(E - E_i(\vec{k})) .$$

In view of the over-all agreement between the EDJDOS and the photoemission spectra, one expects the DOS to be quite reliable. The computed DOS in the d-band region is shown in Fig. 8 plotted on the same energy scale as the structure plot. Within the resolution of the histogram, we note seven peaks in the DOS labeled I–VII. The stronger peaks I, II, IV, V, and VII are located at 2.65, 4.00, 5.05, 6.35, and 7.60 eV, respectively, below the Fermi level. The weaker peaks III and VI are at 4.50 and 6.85 eV below the Fermi level.

The main difference between this DOS and the one calculated previously without spin-orbit coupling is the opening up of a deep trough at about − 6 eV. This divides the d-band DOS into two "clumps" of structure. The upper clump, comprising peaks I, II, III, and VI, extends from about − 5.9 to − 2.2 eV and contains just over six electrons/atom (counting both spins). The lower clump, comprising peaks V–VII, extends from − 8.4 to − 5.9 eV and contains just over four electrons/atom. The separation into upper and lower clumps whose integrated intensities are in the ratio 3 : 2 seems to be consistent with the doublet nature of the x-ray photoemission spectrum reported by Baer *et al.*[25,27] Note that the separation of the two peaks of the doublet should not itself be interpreted as the spin-orbit splitting. Another difference between this DOS and the previous one is the sharp spiky nature of peak V. Further experimental confirmation of this feature is to be found in the photoemission spectrum at $\hbar\omega = 21.2$

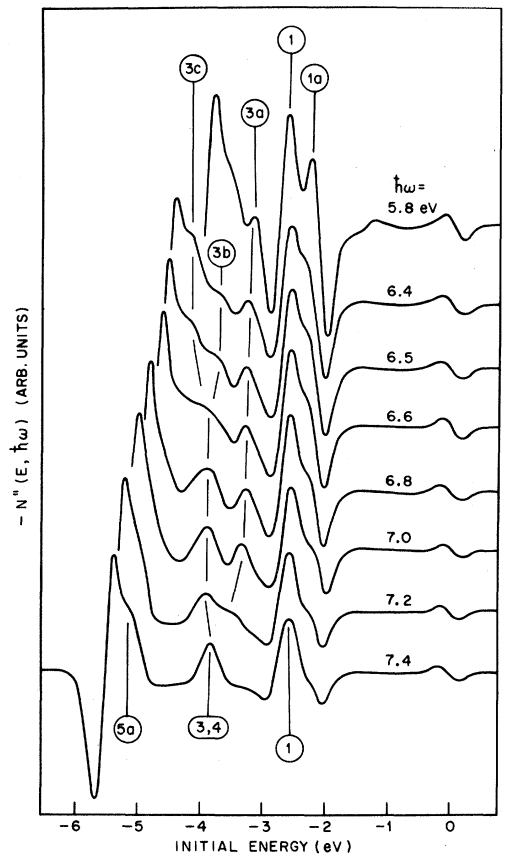

FIG. 7. Experimental higher-derivative photoemission spectra $-N''(E, \hbar\omega)$ taken on cesiated Au in the photon-energy range 5.8–7.4 eV.

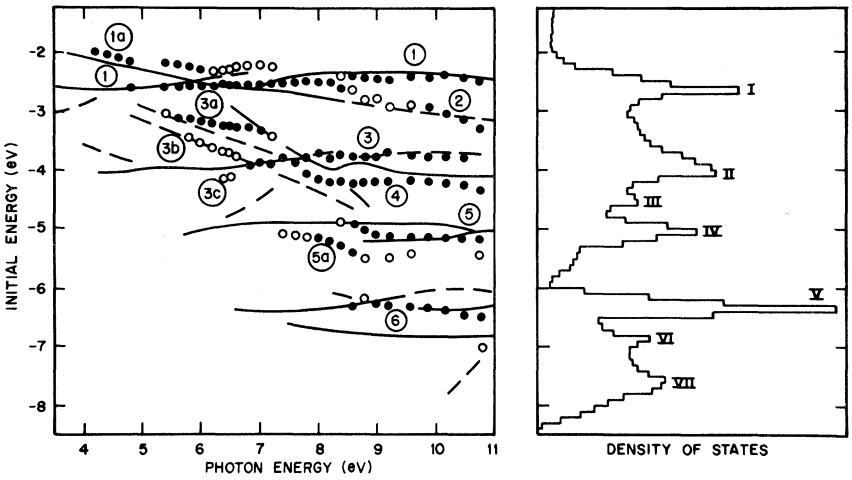

FIG. 8. Comparison of band theory and experiment in Au. The diagram on the left is a structure plot in which the circles denote the energy locations of structure in the experimental $-N''(E, \hbar\omega)$ spectra; full circles represent peaks; open circles represent shoulders. The smooth curves represent the loci of peaks in $-D''(E, \hbar\omega)$ and were constructed by tracing over the contour map of Fig. 5; full lines represent strong peaks and broken curves represent weaker peaks. The figure on the right shows the computed density of states in the d-band region plotted on the same energy scale.

eV reported by Eastman and Cashion.[23]

There is a rough correspondence between structure in the raw spectra and structure in the DOS. For example, in Fig. 8, if we ignore peaks 1a and 2, we see a correspondence between the strong persistent peak labeled 1 in the experimental spectra and peak I in the DOS. Similarly, if we were to draw a horizontal line through the "center of gravity" of the structural complex composed of peaks 3a, 3b, 3c, 3, and 4, it would fall close to peak II in the DOS. We are, however, throwing away a lot of information in order to achieve this correspondence. Likewise, peaks 5 and 6 correspond to peaks IV and V, respectively. Such correspondences are not unexpected. The EDJDOS may be thought of as the density of states over a set of surfaces in $\vec{k}$ space, namely, the surfaces of constant interband energy difference [at least one surface for each pair (i,f) of participating bands]. These surfaces move through $\vec{k}$ space on varying $\hbar\omega$ and, for a sufficiently wide range of $\hbar\omega$, will sweep out a representative volume of the Brillouin zone. It follows that the EDJDOS will, on average, resemble the DOS. There is also the possibility of contributions to the spectra due to nondirect transitions,[16,28] and it may be argued that these should reflect structure in the DOS.[28]

D. Conduction-Band-to-Conduction-Band Transitions

A prominent direct-transition contribution to the photoemission spectra arises from the optical transitions between bands 6 and 7. These start in the vicinity of $L_6^-(L_{2'}) \rightarrow L_6^+(L_1)$ and spread to other parts of the zone on increasing $\hbar\omega$. They give rise to a rectangular box-shaped contribution, to the EDJDOS at the high-energy end of the spectrum,[29] observed previously in the spectra of Cu, Ag, and Au.[4,15,22] This contribution is also clearly observable in the higher-derivative spectra, and we show in Fig. 9 some higher-derivative spectra for Au in the appropriate photon-energy range. The inset of Fig. 9 shows the idealized rectangular box shape for the EDJDOS, $D(E,\hbar\omega)$, and also a

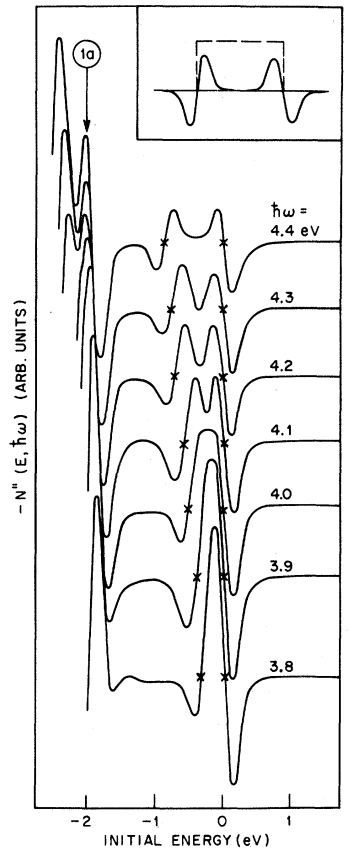

FIG. 9. Experimental higher-derivative spectra $-N''(E, \hbar\omega)$ taken on cesiated Au in the photon-energy range 3.8–4.4 eV. The inset shows the idealized rectangular box shape for the EDJDOS for the optical transitions near L (dashed curve) and also a schematic representation of the smoothed $-D''(E, \hbar\omega)$ curve (full curve).

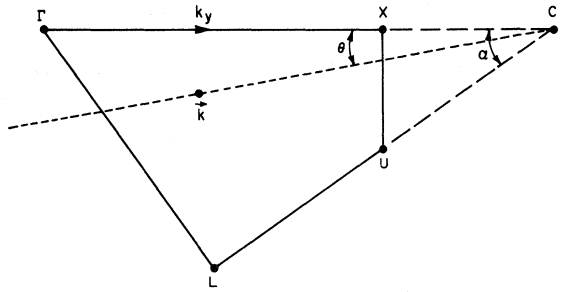

FIG. 10. The ΓXUL plane showing construction used to obtain symmetrizing factors at point $\vec{k}$.

schematic representation of what a smoothed version of $-D''(E,\hbar\omega)$ should look like. The zero crossings in $-D''(E,\hbar\omega)$ are expected to occur close to the edges of the rectangular box. It is seen in Fig. 9 that this characteristic shape is seen at the upper end of the spectrum. The estimated positions of the zero crossings are marked by crosses.

The upper zero crossing falls close to the Fermi level.[4] In a simple two-band model, it has been shown[29] that the energy location of the lower edge of the box should be given by

$$E_{\min} = \frac{(\hbar\omega - E_G)^2}{4E_G} - \frac{V_G^2}{E_G} \quad , \tag{10}$$

where $E_G = \hbar^2 G^2/2m$, and where $\vec{G}$ is one of the $\langle 111\rangle$ reciprocal-lattice vectors and V_G is the corresponding pseudopotential coefficient. A more refined treatment, which takes into account the nonparallelicity of the bands over the hexagonal zone face, has been given by Lindau and Wallden.[24] In either treatment, the $L_6^-(L_{2'}) \rightarrow L_6^+(L_1)$ band gap is given by that photon energy at which the width of the box equals the $L_6^-(L_{2'}) \rightarrow E_F$ separation, which should be about 0.5 eV in order to reproduce the correct radius of the Fermi-surface neck. Taking the zero crossings marked in Fig. 7 as the extremities of the box, we obtain a value of 4.0 eV for the $L_6^-(L_{2'}) \rightarrow L_6^+(L_1)$ band gap. This represents a further small refinement, since the value is marginally smaller than the value of 4.1 eV used in the model band structure described above.

ACKNOWLEDGMENT

The author is very grateful to Morton M. Traum for his assistance with both the experiments and the computer work.

APPENDIX: SYMMETRIZING FACTORS IN HEL SCHEME

In the calculations described in this paper, we have used a modified form for the symmetrizing factors F_2, F_3, and F_4 which appear in the HEL scheme.[5,7] It was found that the expressions for the F's proposed by Ehrenreich and Hodges[5] contain rather rapid variations near some points in $\vec{k}$ space. These in turn bring about small but undesirable kinks in the E-$\vec{k}$ dispersion relations. To remove the kinks we have used the expressions for the F's given in Eqs. (4)–(6). The rationale behind the choice of these particular expressions is discussed below by considering the case of F_3.

F_3 is required to equal 0 at the points Γ and X which happen to define the k_y direction in the particular $\frac{1}{48}$th irreducible sector of the Brillouin zone used here. F_3 is required to equal 1 at the points L, K, U, and W which all lie on the (111) zone boundary. The variation between these values is not too important, although a smooth variation is desirable. Consider the plane ΓXUL of this particular $\frac{1}{48}$th sector as illustrated in Fig. 10. C represents the point of intersection of the lines ΓX and LU. The (111) face of the Brillouin zone is a plane perpendicular to the plane of the paper passing through the line LUC. The dotted line in Fig. 10 represents another plane perpendicular to the plane of the paper and passing through C. This latter plane also contains (k_x, k_y, k_z), the $\vec{k}$-space point under consideration. The angles θ and α are given by

$$\tan\alpha = 2^{-1/2} \quad , \quad \tan\theta = 2^{-1/2}(k_x + k_z)/(12 - k_y) \quad .$$

The functions θ/α or $\tan\theta/\tan\alpha$ will clearly do the job as far as reproducing the correct values of 0 or 1 is concerned. However, they are not the only possibilities. We actually chose

$$F_3 = \sin^2\left(\frac{\pi}{2}\,\frac{\tan\theta}{\tan\alpha}\right) \quad , \tag{A1}$$

which reduces to Eq. (5). The sine-squared form is arbitrary but was chosen in order to ensure slow variations of F_3 in the regions where it is close to 0 or 1. By appropriate construction of planes, F_2 and F_4 may also be expressed in same form, and we obtain Eqs. (4) and (6). It is to be noted that these particular expressions apply only in the correct $\frac{1}{48}$th wedge of the Brillouin zone.

[1]N. E. Christensen and B. O. Seraphin, Solid State Commun. 8, 1221 (1970).
[2]S. Kupratakuln, J. Phys. C Suppl. 3, S109 (1970).
[3]J. W. D. Connolly (unpublished).
[4]N. V. Smith, Phys. Rev. B 3, 1862 (1971).
[5]H. Ehrenreich and L. Hodges, in *Methods in Computational Physics*, edited by B. Alder, S. Fernbach, and M. Rotenberg (Academic, New York, 1968), Vol. 8, p. 149.
[6]N. E. Christensen, Phys. Letters 35A, 206 (1971).

[7]L. Hodges, H. Ehrenreich, and N. D. Lang, Phys. Rev. 152, 505 (1966); L. Hodges, thesis (Harvard University, 1966) (unpublished).
[8]G. C. Fletcher, Proc. Phys. Soc. (London) A65, 192 (1952).
[9]J. Friedel, P. Lenglart, and G. Leman, J. Phys. Chem. Solids 25, 781 (1964); E. Abate and M. Asdente, Phys. Rev. 140, A1303 (1965).
[10]F. Herman and S. Skillman, *Atomic Structure Calculations* (Prentice-Hall, Englewood Cliffs, N.J., 1963).
[11]R. A. Ballinger and C. A. W. Marshall, J. Phys. C 2, 1822 (1969).
[12]k_x, k_y, and k_z are expressed in units in which the distance from Γ to X is 8 units.
[13]The factor $(2\pi)^{-3}$, which appears in previous definitions (Ref. 4), has been dropped. Also, it is understood in Eq. (5) that transitions are considered only if $E_f > E_F > E_i$; i.e., $D(E, \hbar\omega)$ contains an implicit factor $f(E_i)[1-f(E_f)]$, where $f(E)$ is the Fermi function.
[14]D. Brust, Phys. Rev. 139, A489 (1965).
[15]C. N. Berglund and W. E. Spicer, Phys. Rev. 136, A1030 (1964); 36, A1044 (1964).
[16]S. Doniach, Phys. Rev. B 2, 3898 (1970).
[17]W. L. Schaich and N. W. Ashcroft, Phys. Rev. B 3, 2452 (1971); R. M. Broudy, *ibid.* B 3, 3641 (1971); J. G. Endriz and W. E. Spicer, Phys. Rev. Letters 27, 570 (1971).
[18]R. A. Faulkner, in *Computational Methods in Band Theory*, edited by P. M. Marcus, J. F. Janak, and A. R. Williams (Plenum, New York, 1971), p. 16.
[19]E. O. Kane, Phys. Rev. 175, 1039 (1968).
[20]W. E. Spicer and C. N. Berglund, Rev. Sci. Instr. 35, 1665 (1964).
[21]N. V. Smith and M. M. Traum, Phys. Rev. Letters 25, 1017 (1970).
[22]P.-O. Nilsson, C. Norris, and L. Walldén, Physik Kondensierten Materie 11, 220 (1970).
[23]D. E. Eastman and J. K. Cashion, Phys. Rev. Letters 24, 310 (1970).
[24]I. Lindau and L. Walldén, Physica Scripta 3, 77 (1971).
[25]A more detailed comparison of the EDJDOS calculated with and without spin-orbit coupling has been presented by N. V. Smith and M. M. Traum, in Proceedings of the International Colloquium on Electron Spectroscopy (unpublished). The effects in x-ray photoemission spectra are also considered.
[26]V. Heine, Phys. Rev. 153, 673 (1967); J. C. Phillips, Advan. Phys. 17, 79 (1968).
[27]Y. Baer, P. F. Hedén, J. Hedman, M. Klasson, C. Nordling, and K. Siegbahn, Physica Scripta 1, 55 (1970).
[28]W. E. Spicer, Phys. Rev. 154, 385 (1967); W. F. Krolikowski and W. E. Spicer, Phys. Rev. B 1, 478 (1970).
[29]R. Y. Koyama and N. V. Smith, Phys. Rev. B 2, 3049 (1970); see also S. Methfessel, Z. Physik 147, 442 (1957).

PHYSICAL REVIEW B VOLUME 5, NUMBER 4 15 FEBRUARY 1972

Magnetic Surface Levels in Antimony in a Tipped Magnetic Field*

S. P. Singhal and R. G. Goodrich
Department of Physics and Astronomy, Louisiana State University, Baton Rouge, Louisiana 70803
and
R. C. Jones†
Department of Physics, Southwestern State College, Weatherford, Oklahoma 73096
(Received 26 April 1971; revised manuscript received 20 September 1971)

The tip effect for the low-field surface-state resonances is studied for antimony. A theoretical expression for the position of surface-state peaks arising from a cubic Fermi surface is derived. The experimental results give qualitative agreement with the theory and check the validity of the approximation that allows the replacement of $\vec{p}$ by $\vec{p} - e\vec{A}/c$ in the Hamiltonian in the presence of a magnetic field.

I. INTRODUCTION

In a recent paper,[1] hereafter referred to as SP, the energy levels and the wave functions for electrons skipping along a surface in a magnetic field were studied theoretically for a general orientation of magnetic field and sample surface relative to the crystal axes of the material. It was concluded that in the case of a quadratic Fermi surface (FS), the results were generally the same as those for a field parallel to the sample surface, as long as the normal component of the applied field was "small." The "smallness" criterion is $\omega_z \tau \ll 1$, where ω_z is the local cyclotron frequency for the normal component of the field. Some qualitative remarks were made in SP for the case of a general FS. In the present paper, the tip effect for the case of a cubic FS is derived and experimental results for antimony are given.

As mentioned in SP, it is expected that the main contribution to the surface-state resonances comes from the vicinity of the point on the FS where $\epsilon_n - \epsilon_m$ is extremal with respect to p_y (where p_x is considered to be a function p_y). This condition was given by SP to be that the function Q, given by

$$Q = \frac{(\vec{V}\times\vec{B})_3}{\sqrt{m_3}}\left(1 - \frac{\vec{B}\cdot\overleftrightarrow{m}\cdot\vec{\Gamma}}{\vec{B}\cdot\overleftrightarrow{m}\cdot\vec{B}}B_3\right), \quad (1)$$